RSC Advances

ROYAL SOCIETY OF CHEMISTRY

www.rsc.org/advances

Journal Name

ARTICLE

Fast electrodeposition, affecting factors and catalytic properties of dendritic Cu-M (M = Ni, Fe, Co) microstructures

Received 00th January 20xx,
Accepted 00th January 20xx

DOI: 10.1039/x0xx00000x

www.rsc.org/

Huying Zhang, Yonghong Ni*, Yiman Zhong, Hao Wu and Muheng Zhai

Rapid electrochemical deposition of dendritic Cu-M (M = Ni, Fe, Co) microstructures with excellent catalytic activity was reported here. Simple Cu^{2+} and M^{2+} salts were employed as the initial metal sources and boric acid as the buffer solution. The electrodeposited process was carried out at the deposition current of 10 mA for 5 min in air at room temperature. The phase and morphology of the as-prepared products were characterized by field emission scanning electron microscopy (FESEM), powder X-ray diffraction (XRD), energy dispersive spectrometry (EDS) and transmission electron microscopy (TEM). It was found that the formation of dendritic Cu-M microstructures could be affected by some factors including the amounts of M^{2+} salts and boric acid, and the deposited current and time. As a representative, the performances of Cu-Ni dendrites were studied. The investigations showed that the as-deposited Cu-Ni dendrites exhibited good electrochemical responses in 0.1 M KOH solution and could be used as an electrochemical catalyst for the reduction of nitrate and the oxidation of glucose. Also, the as-deposited Cu-M dendrites exhibited excellent catalytic activities for the reduction of 4-nitrophenol to 4-aminophenol in excess $NaBH_4$ solution.

1. Introduction

Since the properties of nanomaterials can be tuned by their sizes and shapes, it is of significant realizing the controllable syntheses of nanomaterials. Compared with other structures, generally, branched nanostructures have the larger surface areas, allow for heterostructures and can easily form continuous networks. Hence, the preparation of dendritic micro/nanostructures has been paid much attention over the past decade.[1] Many methods have been developed, including the hydrothermal method,[2] the template-assisted route,[3] the laser-driven growth,[4] the rapid circumfluence synthesis,[5] the electrochemical deposition,[6] the wet chemical approach,[7] and so on. Among them, the electrodeposition technology is a simple, fast and energy-efficient method. Also, the electrodeposited process of dendrites can be carried out at ambient pressure and temperature, requiring relatively inexpensive equipment compared with other methods. Employing this technology some element and compound dendrites have been successfully obtained in our groups.[8]

Transition metal elements, especially iron, cobalt and nickel, always attract extensive research interest in materials science due to their outstanding physiochemical, mechanical, magnetic and catalytic performances, and as well wide applications in many fields. With the development of nano-science/technology, Fe, Co, Ni and their alloys with various morphologies have been obtained through a variety of methods.[9] As an element following nickel, copper also draws much attention owing to its wide commercial applications in verities of fields as heat transfer materials, antimicrobial materials, super strong materials, sensors and catalysts, etc.[10] Furthermore, Cu can easily form alloys with many metals including Fe, Co and Ni; and Cu-M (M = Fe, Co and Ni) micro/nano-structures exhibit special magnetic or magnetoresistive properties.[11] Recently, nanostructural Cu-Ni alloys with various atomic ratios are drawing much attention because of their excellent catalytic activity for nitrate reduction, furfural hydrogenation, and methane reforming with CO_2.[12-18] For example, Mattarozzi and coworkers deposited Cu-Ni alloys from a single citrate bath through a potentiostatic mode and found that the as-obtained Cu-Ni alloys presented superior performances in the reduction of nitrate and nitrite than pure Cu and Ni.[19] Subsequently, a hydrogen evolution assisted potentiostatically-electrodeposited route was also employed for the preparation of porous Cu-Ni alloy foams, which exhibited outstanding performances including large stable currents, and fast and selective nitrate reduction to ammonia.[18] Similarly, Zhang et al also potentiostatically deposited Cu-Ni foam films and investigated the magnetic property and superhydrophobicity of the porous films. Experiments showed that Cu-Ni porous films displayed superior stability and enhanced electrocatalytic activity for

[a] College of Chemistry and Materials Science, Key Laboratory of Functional Molecular Solids of Ministry of Education, Anhui Laboratory of Molecule-Based Materials, Anhui Key Laboratory of Functional Molecular Solids, Anhui Normal University, Wuhu, 241000, PR China. E-mail: niyh@mail.ahnu.edu.cn

hydrogen evolution reduction than pure Cu and Ni porous films.[20]

Different from the above potentiostatic deposition, in this work, we designed a simple galvanostatic deposition route to prepare dendritic Cu-M (M = Fe, Co and Ni) microstructures from a H_3BO_3 solution under ambient conditions, employing $CuCl_2$ and MCl_2 as the initial metal sources. Some factors affecting the formation of dendritic Cu-M microstructures were systematically investigated, including the deposition time, the amounts of M^{2+} salts and boric acid, and the deposition current. Experiments showed that the presences of M^{2+} salts played crucial roles in the formation of dendritic Cu-M microstructures. Moreover, the performance tests showed that the deposited dendritic Cu-M microstructures presented excellent catalytic activities for the reduction of 4-nitrophenol (4-NP) to 4-aminophenol (4-AP) in excess $NaBH_4$ solution. It was found that dendritic Cu-Ni microstructures still presented outstanding electrocatalytic abilities for the reduction of nitrate ion (NO_3^-) to ammonia (NH_3) and the oxidation of glucose in KOH solution, respectively.

2. Experimental

All reagents and chemicals are analytically pure, bought from Shanghai Chemical Company and used without further purification.

2.1 The deposition of dendritic Cu-M microstructures

In a typical experiment, a conventional three-electrode cell was used, employing a Pt wire as the counter electrode, a saturated Ag/AgCl electrode as the reference electrode, and a conductive ITO (Indium-Tin Oxide) glass with a size of 1 × 3 cm^2 as the working electrode. Before the experiment, the ITO electrode was in turn treated by ultrasounds for 30 min in acetone, ethanol and twice-distilled water, and then dried at room temperature. To obtain dendritic Cu-M microstructures, 1 mmol of $CuCl_2$ was firstly dissolved in a certain amount of twice-distilled water. Then, 9 mmol MCl_2 (M = Fe, Co and Ni) and 1 mmol of H_3BO_3 were introduced to the above solution. Subsequently, the system was diluted to 30 mL by adding twice-distilled water. Here, the concentrations of Cu^{2+}, M^{2+} and H_3BO_3 were in turn 0.033, 0.3 and 0.033 mol L^{-1}. Finally, the electrodeposited experiments were conducted at a deposition current of 10 mA for 5 min in air at room temperature.

2.2 Characterization

The X-ray diffraction (XRD) patterns of the electrodeposited products were recorded on a Shimadzu XRD-6000 X-ray diffractometer (Cu Kα radiation, λ=0.154060 nm), employing a scanning rate of 0.02°/s and 2θ ranges from 30° to 80°. Field emission scanning electron microscopy (FESEM) images and energy dispersive spectra (EDS) of the final products were taken on a Hitachi S-4800 field emission scanning electron microscope, employing an accelerating voltage of 5 or 15 kV (15 kV for EDS). High resolution transmission electron microscopy (HR/TEM) images were recorded on a FEI Techna G^{20} transmission electron microscope, employing an accelerating voltage of 200 kV. X-ray photoelectron spectroscopy (XPS) of the product was obtained on Thermo ESCALAB 250 instrument, employing monochromic Al Kα (hν =1486.6 eV) at the power of 150 W.

2.3 Performance tests

To investigate the catalytic property of the as-deposited dendritic Cu-M microstructures for the reduction of 4-nitrophenol (4-NP) to 4-aminophenol (4-AP), a series of solutions was freshly prepared before the experiment. Firstly, a certain amount of catalyst was dispersed into small amounts of 4-NP solution. Then, $NaBH_4$ solution was introduced into the above system. The total volume of the system was tuned to 3 mL. Here, the concentrations of 4-NP, $NaBH_4$ and catalyst were 1.0×10^{-4} mol L^{-1}, 2×10^{-2} mol L^{-1} and 4 mg L^{-1}, respectively. The reduction processes were monitored with a Metash 6100 UV-vis spectrophotometer.

Simultaneously, to investigate the electrochemical properties of Cu-Ni dendrites for the reduction of NO_3^- to NH_3 and the oxidation of glucose to gluconolactone in KOH solution, a Ag/AgCl electrode (in saturated KCl, aq.) was selected as the reference electrode, Platinum coil (0.5 mm × 4 cm) as the counter electrode and a modified glass carbon electrode (GCE) as the working electrode. The working electrode was prepared as follows: Firstly, a GCE was polished in 1700# diamond paper with 1 mm, 0.3 mm, 0.05 mm alumina in turn, and washed successively with 0.1 M HNO_3 and ethanol in an ultrasonic bath. Secondly, 1 mg of the dendrite was dispersed into 1 mL of twice distilled water under sonication. Next, 5 μL of the dendrite solution was dropped onto the surface of the GCE. Subsequently, 3 μL of 0.5 wt% Nafion solution was dropped on the surface to tightly attach the dendrite onto the surface of the electrode. Thus, the GCE modified by Cu-Ni dendrites was obtained. The reduction process of NO_3^- to NH_3 and the oxidation process of glucose to gluconolactone were monitored with a computer-controlled CHI660D electrochemical workstation.

3. Results and discussion

3.1 Morphology and structure characterization

Figure 1 shows the representative FESEM images of the products deposited from $CuCl_2$-H_3BO_3 systems without and with M^{2+} salts (M = Fe, Co or Ni) under the present experimental conditions. Obviously, when the system did not contain M^{2+} salts, no dendrite was deposited (see Fig.1a). After introducing M^{2+} salts into the system, dendritic microstructures were obtained (see b, c and d in Fig.1). Namely, the presence of M^{2+} salts caused the growth of dendritic microstructures under the current electrodeposited conditions. Since the deposited products could be moved by a magnet, magnetic matters should be produced in the present electrodeposition process. Considering the system composition and the electro-reduction condition, it was possible that the deposited products contained magnetic metal, Fe, Co or Ni. Figure 2 (a-c) depict the EDS analyses of the products deposited from $CuCl_2$-H_3BO_3 systems with M^{2+} salts (M = Fe, Co or Ni). Besides Cu peak, strong Fe,

Co or Ni peaks are also detected in the samples, respectively, indicating that the final products contain Fe, Co or Ni indeed. However, according to the calculation of the peak area, the Cu/M molar ratio is almost 4/1 for Cu/Co, 2/1 for Cu/Fe, and 1/3 for Cu/Ni (see the inserts in Fig.2 (a-c)). The above facts imply that the deposited amounts of magnetic metals are different under the same electrodeposited conditions owing to the difference of the original metal source. Furthermore, the amount of C element is close in three samples, which should be attributed to the double-sided-tape. However, the amounts of O element are different from each other. The amount of O element in Cu-Fe sample is the highest, then Cu-Co, finally Cu-Ni. The above phenomena are understandable. In the light of the standard potentials, the reductive ability of Fe (E^o = −0.44 V NHE), Co (E^o = −0.28 V NHE) and Ni (E^o = −0.25 V NHE) weakens in turn. Nanosized Fe is easily oxidized in air, then Co, and Ni is the most stable. Hence, the amount of O element is different in three samples. Figure 2d depicts the XRD patterns of products. According to the order of Co, Fe, Ni, the intensities of cubic Cu peaks gradually weaken and those of M peaks increase, indicating that the amount and the crystallinity of M increase in turn. The above result is in good agreement with the Cu/M molar ratio (see the inserts in Fig.2 (a-c)). However, no obvious Co peak is detected in the Cu-Co sample, implying that a small amount of Co was deposited. In 1998, Bakkaloğlu et al found that the diffraction peak of Co could not be detected from Cu-Co alloy films with the cobalt content from 6% to 26%.[21] Based on the calculation of EDS, ~20% Co existed in the present Cu-Co sample. Thus, no obvious Co peak is detected in the Cu-Co sample.

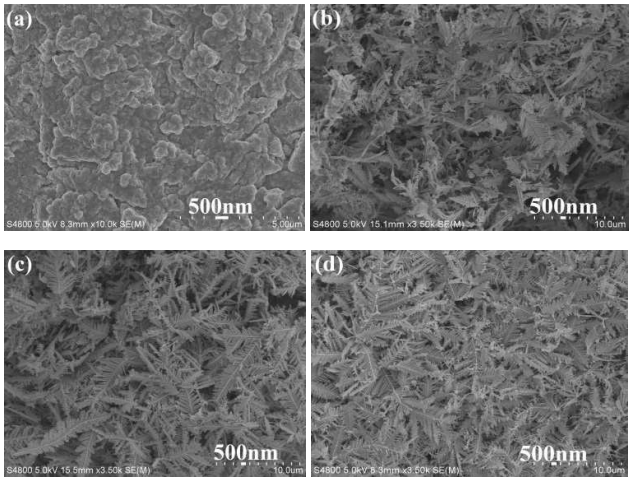

Figure 1 FESEM images of the samples deposited from $CuCl_2$-H_3BO_3 systems without and with M^{2+} (M = Fe, Co and Ni) salts at the deposition current of 10 mA for 5 min in air at room temperature: (a) without M^{2+} ions, (b) with Fe^{2+} ions, (c) with Co^{2+} ions and (d) with Ni^{2+} ions.

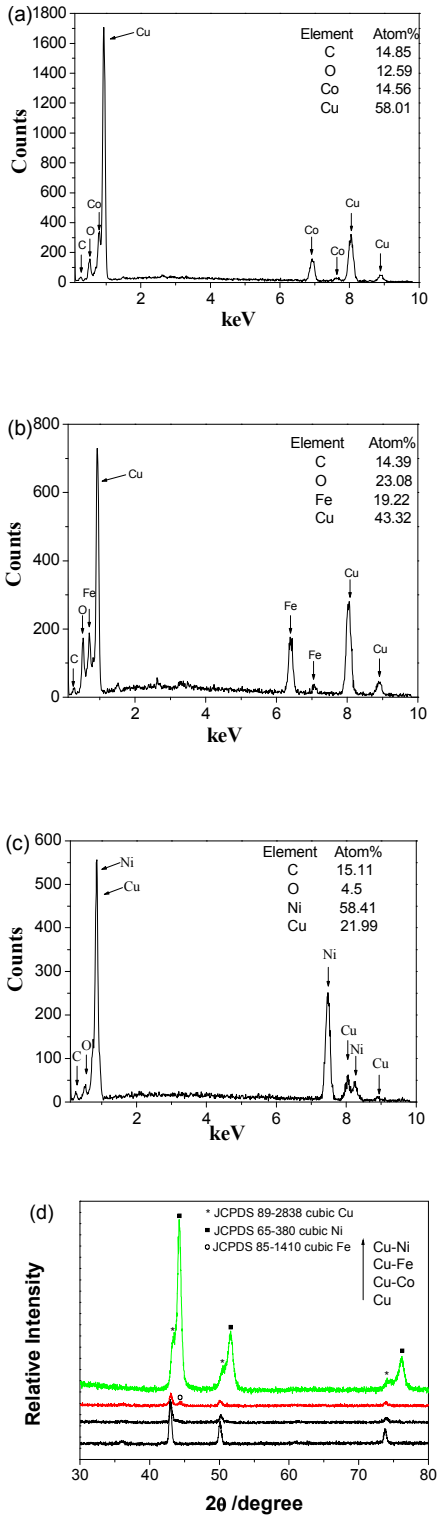

Figure 2 (a-c) EDS analyses and (d) XRD patterns of the products deposited $CuCl_2$-H_3BO_3 systems with M^{2+} (M = Fe, Co and Ni) salts at the deposition current of 10 mA for 5 min in air at room temperature.

To further ascertain the existence state of M in the surface of Cu-M alloy, the XPS technology was employed. As shown in Figs. 3a and 3b, no Fe(0) and Co(0) are detected.[22,23] However, Ni(0) peak can still be detected in Cu-Ni sample (see Fig.3c).[24] The above facts indicated that Fe and Co elements in the surfaces of Cu-Fe/Co samples had been oxidized and Ni element was only partially oxidized.

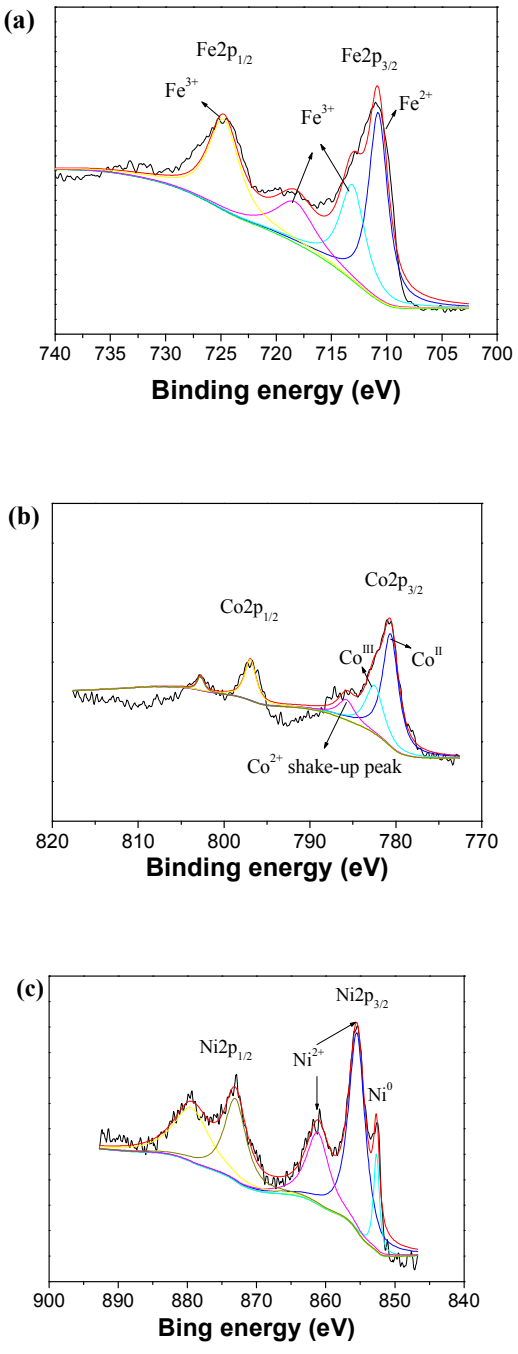

Figure 3 high resolution XPS of Fe (a), Co (b) and Ni (c) in three samples.

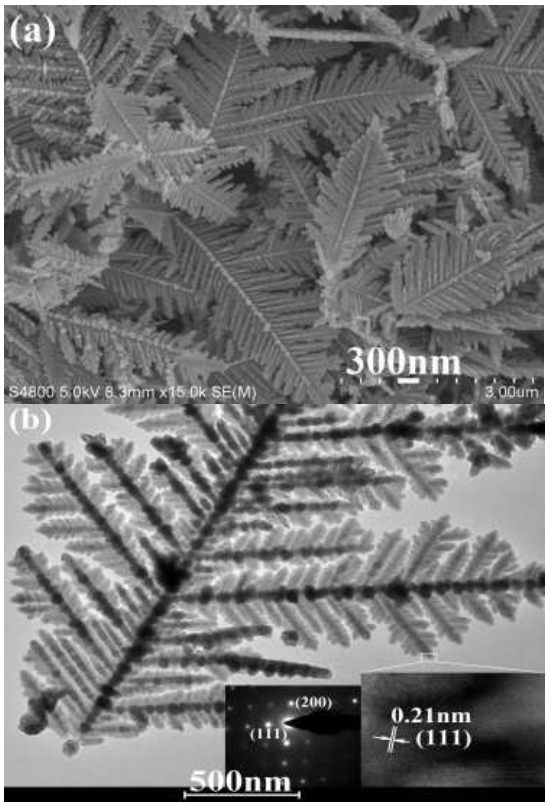

Figure 4 (a) High magnification FESEM image and (b) TEM image of Cu-Ni dendrites deposited from the system with 1 mmol of $CuCl_2$, 9 mmol $NiCl_2$ and 1 mmol H_3BO_3 at the deposition current of 10 mA for 5 min. The insets in (b) are in turn SAED pattern and HRTEM image of the stem.

Here, Cu-Ni dendrites are selected as the representative for further investigation since Ni is more stable than Fe and Co. **Fig.4a** depicts a high-magnification FESEM image of Cu-Ni dendrites, from which some sub-branches of dendrites are clearly visible. TEM observations further prove the dendritic structure of Cu-Ni sample. As shown in **Fig.4b**, all stems are constructed by nearly-spherical nanoparticles with a mean size of ~50 nm, like knotted straight strings. The sub-branches grow from these knots and almost parallel to each other. Similar phenomena were also found during the electrodeposition process of PbTe.[25] The right inset in **Fig.4b** shows a HRTEM image of the tip in a stem. Clear lattice fringes imply good crystallinity of dendritic structures. The d-spacing value of neighbouring planes is calculated to be ~0.21 nm, which is close to the (111) plane of Cu (Ni). The corresponding SAED pattern confirms the single crystal nature (see the left inset in **4b**).

3.2 Affecting factors

3.2.1 The amounts of original $NiCl_2$ and boric acid

In the present system there were only three components except the solvent: $CuCl_2$, $NiCl_2$ and H_3BO_3. Keeping the amount of $CuCl_2$ constant, experiments uncovered that the amounts of original $NiCl_2$ and boric acid could markedly affect the morphology of Cu-Ni microstructures.

Figure 5 exhibits typical FESEM images of the products deposited from the systems with different amounts of original $NiCl_2$. Dendritic structures can be always obtained under the same deposition conditions and with the increase of the original $NiCl_2$ amount, the sizes of dendrites gradually increase. Nevertheless, the dendrites gradually become perfect with the increase of the $NiCl_2$ amount from 0.1 mmol to 9 mmol; then, retrograde from 9 mmol to 15 mmol. Namely, 9 mmol of $NiCl_2$ is the optimum amount in the formation of perfect Cu-Ni dendrites.

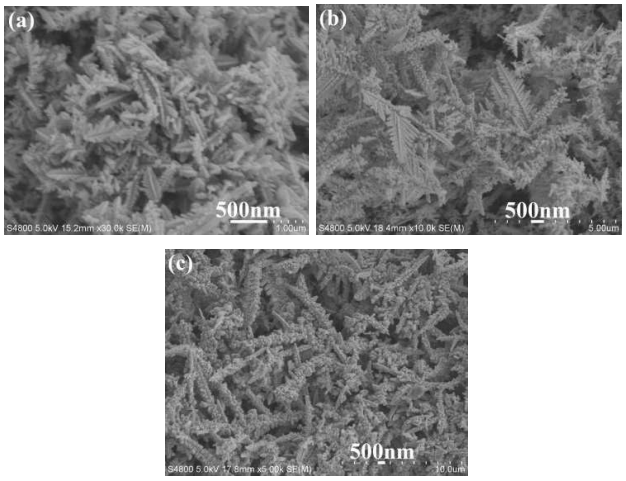

Figure 5 FESEM images of Cu-Ni **microstructures** deposited at the deposition current of 10 mA for 5 min from the systems with various amounts of $NiCl_2$: (a) 0.1 mmol, (b) 2 mmol and (c) 15 mmol.

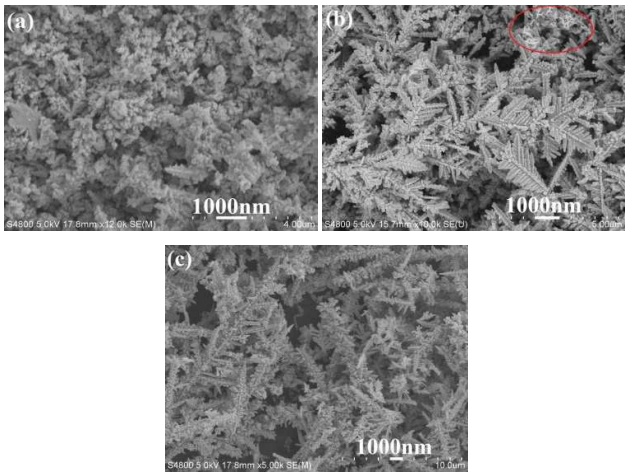

Figure 6 FESEM images of Cu-Ni **microstructures** deposited at the deposition current of 10 mA for 5 min from the systems containing different amounts of H_3BO_3: (a) 0 mmol, (b) 0.5 mmol and (c) 3 mmol.

As a buffering reagent, boric acid is often used during the electrodeposition. In the present system, when no boric acid was used, the deposited product consisted of abundant irregular particles and few immature dendrites under the same experimental conditions (see **Fig.6a**). After 0.5 mmol of boric acid was introduced into the system, the product almost presented dendritic microstructures **(see Fig.6b)** except few sheet-like particles **(see the red circle in 6b**). After 1 mmol of boric acid was employed, a great deal of perfect dendrites was obtained (see Fig.1d and **Fig.4**). Upon further increasing the amount of boric acid, for example to 3 mmol, the dendrites ceaselessly grew up. Meanwhile, the sub-structures of dendrites gradually lost **(see Fig.6c)**. Namely, perfect dendritic-structures retrograded with the amount increase of boric acid. The above facts clearly showed that the amount of boric acid also played an important role in the formation of perfect Cu-Ni dendrites. Some studies have uncovered that boric acid could lower the over-potential and increase the current efficiency, which promoted the electrodeposition of metals.[26,27] Recently, Graham et al investigated the role of boric acid in the formation of Ni nanotubes under the AAO template assisted electrodeposition conditions and believed that a nickel-borate complex formed between Ni^{2+} and borate ions acted as the crucial role in the formation of Ni nanotubes.[27] Also, their research discovered that the concentration of boric acid could tune the wall thickness of nanotubes.[27] In the present work, obviously, metal-borate complexes could be formed, too. Under the same electrochemical conditions, the deposition of metal (Fe, Co and Ni) was promoted. Within the same deposition time, more metal particles were produced. The previous-produced metal nuclei became the seeds for further growth of the freshly deposited particles. Since borate ions (or boric acid molecules) still existed in the surroundings of deposited metal nuclei, it was possible that they affected the nucleation and growth of the product. Namely, boric acid probably acted as the structure-directing reagent, too. As a result, dendritic Cu-Ni microstructures were obtained.

3.2.2 The deposition time

To further ascertain the growth process of Cu-Ni dendrites, a time-dependent shape evolution experiment was designed. As shown in **Fig.7a** and its inset, few flowerlike microstructures were scattered in abundant small particles after depositing for 30 s. After 1 min, certain petals of micro-flowers rapidly grew to form dendritic microstructures. Simultaneously, more small particles also grew into new flowerlike microstructures (see **Fig.7b**). Dendritic microstructures continuously grew up with the prolongation of the deposition time. After depositing for 3 min, dendritic microstructures became the main product (see **Fig.7c**). When the deposition time of 5 min was employed, a plenty of perfect dendrites was obtained (see Fig.1d and **Fig.4**). Hereafter, the shape of the product gradually retrograded with the expansion of the deposition time. For example, **Fig.7d** displays a typical FESEM image of the product deposited at the current of 10 mA for 10 min. Dendritic microstructures are still clearly visible, but the sizes become bigger and sub-branches coarsen compared with those deposited for 5 min.

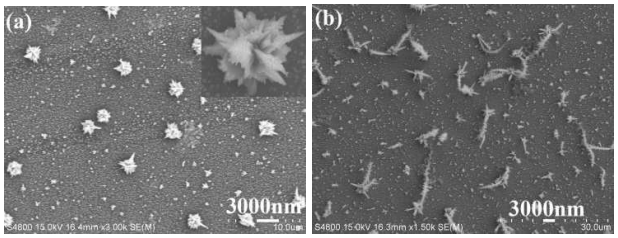

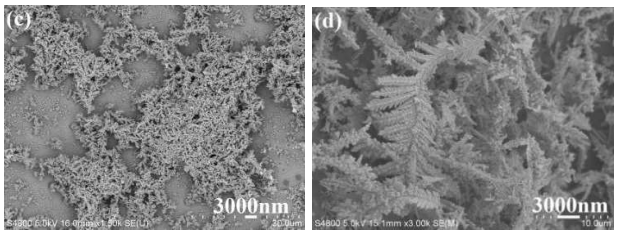

Figure 7 FESEM images of Cu-Ni **microstructures** deposited under the same conditions for different durations: (a) 30 s, (b) 1 min, (c) 3 min and (d) 10 min.

The above shape evolution experiment clearly showed the formation process of dendritic microstructures. In the initial stage, abundant small particles were firstly obtained and acted as the seeds for further growth. Subsequently, flowerlike microstructures were rapidly formed. With the expansion of the deposition time, the flowerlike microstructures ceaselessly grew along certain directions owing to their high surface energies. Thus, dendritic microstructures started to appear and gradually tended to perfect. With the proceeding of the deposition process, however, perfect dendrites gradually retrograded, which should probably be attributed to the growth rate change of various crystal-planes.

3.2.3 The deposition current

Furthermore, it was found that the deposition current could also affect the morphology of the product. **Fig.8** shows the representative FESEM images of the products deposited from the same system at the deposition current of 5 mA and 20 mA for 5 min, respectively. Compared with FESEM images shown in Fig.1d, dendritic microstructures can be still obtained, but the dendrites obtained at 20 mA present the bigger sizes and markedly retrograde. Namely, the bigger deposition current is unfavourable to the growth of perfect dendrites. This is understandable. When the other conditions are kept constant, the deposition rate increases with the increase of the deposition current. Since the nucleation and growth rates of the product are determined mainly by the deposition rate, more products will be deposited under the higher deposition current within the same time. Simultaneously, the nucleation and growth rates increase, which lead to the morphology change of the final product in the present work.

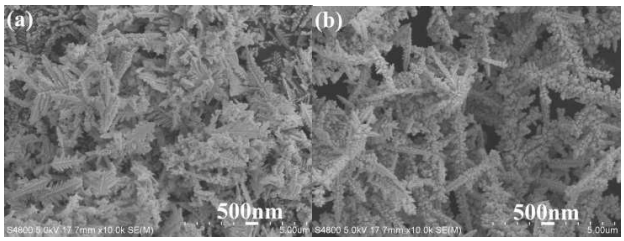

Figure 8 FESEM images of Cu-Ni **microstructures** deposited from the system with 1 mmol $CuCl_2$, 9 mmol $NiCl_2$ and 1 mmol H_3BO_3 at various currents for 5 min: (a) 5 mA and (b) 20 mA.

In 1963, Brenner pointed out that the electrodeposition of alloys containing one or more of iron, cobalt or nickel often took place at the anomalous codeposition mode, which is characterized by the anomaly that the less noble metal deposits preferentially.[28] In the present system, the concentration of M^{2+} ions (M = Fe, Co or Ni) was 9 times than that of Cu^{2+} ions. The redox potential of M^{2+}/M pair was calculated to be in turn 0.296 V for Cu^{2+}/Cu, -0.265 V for Ni^{2+}/Ni, -0.295 V for Co^{2+}/Co and -0.455 V for Fe^{2+}/Fe. Markedly, Cu^{2+}/Cu pair bears far higher redox potential than M^{2+}/M pair. Less Cu^{2+} ions should be deposited prior to M^{2+} ions. Namely, the electrodeposition of the present Cu-M systems should comply with the above anomalous codeposition mode. Thus, Cu-M dendrites were finally deposited.

3.3 Properties of Cu-M microstructures

3.3.1 Catalytic activities for the reduction of 4-nitrophenol

To investigate the catalytic activities of Cu-M (M = Fe, Co and Ni) dendrites, the reduction of 4-nitrophenol (4-NP) by excess $NaBH_4$ to 4-amiophenol (4-AP) in aqueous solution was used as the mode reaction. Generally, 4-NP solution has a strong absorption peak at 317 nm and a weak shoulder peak at 400 nm in the region of 250 ~ 550 nm (see the thick curve in **Fig.9a**). However, the absorption peak at 317 nm will disappear after alkali $NaBH_4$ is added into 4-NP solution. Here, only one peak at 400 nm exists and the peak intensity markedly increases, which should be attributed to the production of the intermediate state, 4-nitrophenolate ion.[29] If a catalyst is introduced into the above system, the peak at 400 nm gradually decreases; and concomitantly, a new peak at ~305 nm appears due to the production of 4-AP.[30] **Figs.9(a-c)** show the UV-vis absorption spectra of 4-NP-$NaBH_4$ system in the presence of 4 mg L^{-1} Cu-M dendrites at various reactive durations. With the prolonging of the reaction time, the peak at 400 nm decreases, indicating good catalytic activities of the as-deposited Cu-M dendrites for the reduction of 4-nitrophenol (4-NP) to 4-amiophenol (4-AP) in excess $NaBH_4$ solution. **Fig.9d** depicts the linear relationships between $ln(C_t/C_0)$ and the reaction time in the presences of the as-deposited Cu-M dendrites. Here, C_0 and C_t separately stand for the concentration of 4-NP at the initial stage and certain reaction time. The corresponding rate constants are calculated to be 0.83 min^{-1} for Cu-Ni, 0.69 min^{-1} for Cu-Fe and 0.48 min^{-1} for Cu-Co, respectively.

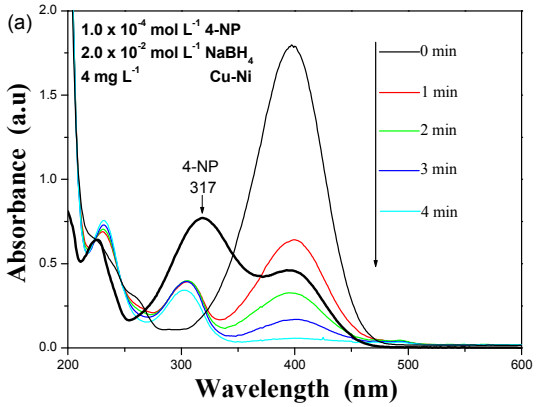

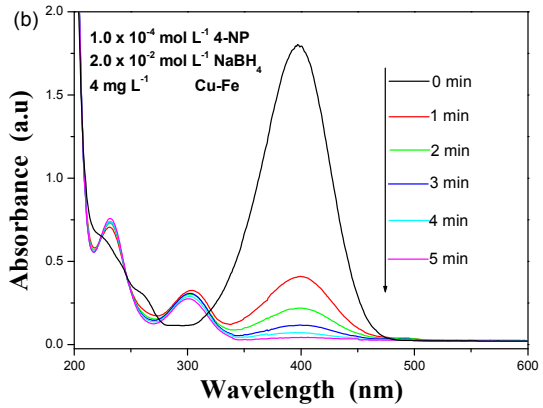

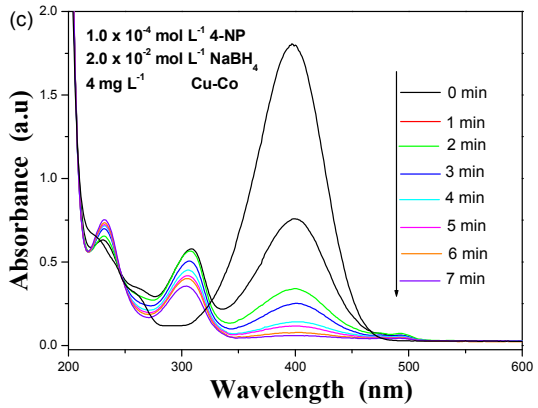

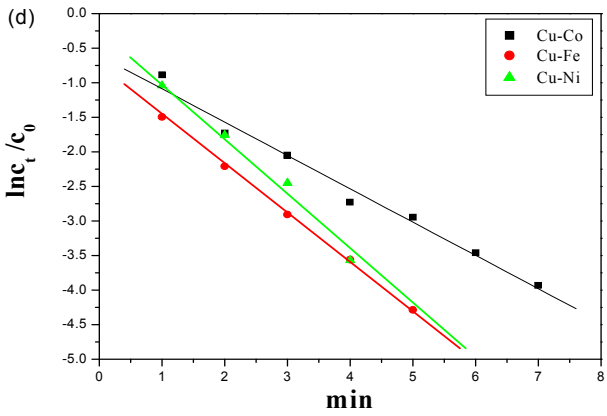

Figure 9 (a-c) The UV-vis absorption spectra of 4-NP-$NaBH_4$ system in the presence of 4 mg L^{-1} Cu-M dendrites at various reactive durations: (a) Cu-Ni, (b) Cu-Fe and (c) Cu-Co. (d) The linear relationships between $\ln(C_t/C_0)$ and the reaction time in the presences of 4 mg L^{-1} Cu-M dendrites.

Fig.10a depicts the histograms of the catalytic efficiencies of Cu-M catalysts *vs* cycle times. After cycling for 5 times, the catalytic efficiency of Cu-Fe dramatically decreases; the one of Cu-Co evidently reduces and the one of Cu-Ni slightly decreases. Namely, Cu-Ni microstructures bear better catalytic stability than Cu-Fe/Co **ones. Figs. 10b-10d** display FESEM images of Cu-M catalysts after 5 cycles, separately. Comparing with those shown in Figs. 1b-1d, one can find that the shapes of Cu-Fe/Co obviously retrograde and the shape of Cu-Ni hardly changes. The above facts indicate that the catalytic efficiencies of Cu-M catalysts are related to the morphologies of Cu-M microstructures.

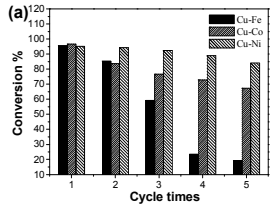

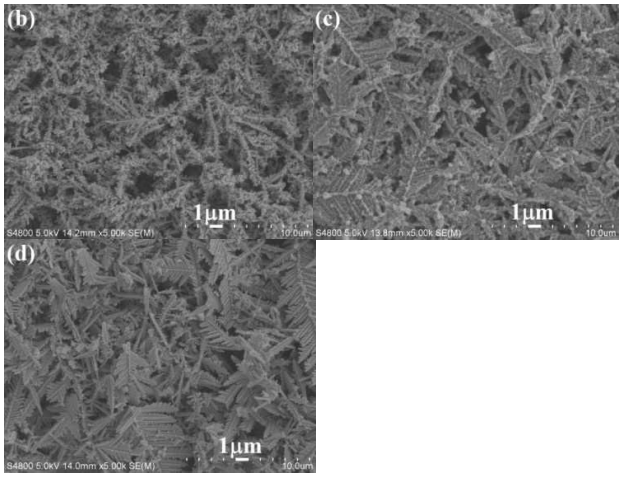

Figure 10 (a) the histograms of the catalytic efficiencies of Cu-M catalysts *vs* cycle times; and FESEM images of Cu-M catalysts after 5 cycles: (b) Cu-Fe, (c) Cu-Co and (d) Cu-Ni.

3.3.2 Electrocatalytic activity

It was found that the present Cu-Ni dendrites also displayed excellent electrochemical activities for catalytic reduction of NO_3^- ions and oxidation of glucose. **Fig.11a** depicts CVs of Cu-Ni dendrites-modified GCE in 1 M KOH solution and the mixed solution of 1 M KOH + 1 M KNO_3 at scan rate of 100 mV s^{-1}, respectively. A pair weak redox peak can be seen in 1 M KOH solution; and a pair strong redox peak appears in the mixed solution of 1 M KOH + 1 M KNO_3. Also, their peak sites are different from those in 1 M KOH solution. Obviously, the presence of KNO_3 causes the change of the redox peak. Mattarozzia's studies had confirmed that Cu-Ni alloys could catalyze the reduction of NO_3^- ions to NH_3 in the alkaline medium.[18,19] Since the current catalytic experiments were carried out under the same conditions used in Mattarozzia's studies, the present Cu-Ni dendrites also owned excellent catalytic activity for the reduction of NO_3^- ions to NH_3 in the alkaline medium. **Fig.11b** shows the CVs of Cu-Ni/Nafion/GCE in the mixed solution of 1 M KOH + 1 M KNO_3 at the scan rates of 10~100 mV s^{-1}. It can be seen that the Cu-Ni/Nafion/GCE presents the well-defined redox peaks at the different scan rates, which should be assigned to the Ni^{III}/Ni^{II} redox couple in alkaline medium.[18,19,31] Moreover, with the increase of the scan rate from 10~100 mV s^{-1}, both cathodic and anodic peak currents linearly increase with the square root of

the scan rate (see the insert in **Fig.11b**), which reveals the diffusion controlled electrochemical process of the electron transfer on the Cu-Ni/Nafion/GCE. Mattarozzia et al considered that the electrocatalytic activity of Cu-Ni alloys for the reduction of NO_3^- ions should be attributed to the synergistic effect between Cu and Ni.[18,19] In alloys, Cu sites well adsorbed NO_3^- ions and Ni sites efficiently adsorbed H atoms produced by the discharge of H_2O molecules. Subsequently, the reductive reaction was initiated through the transfer of adsorbed H atoms. The reductive reaction can be simply described as follows: [18,19]

$$NO_3^- + 6H_2O + 8e^- \rightarrow NH_3 + 9OH^- \quad (1)$$

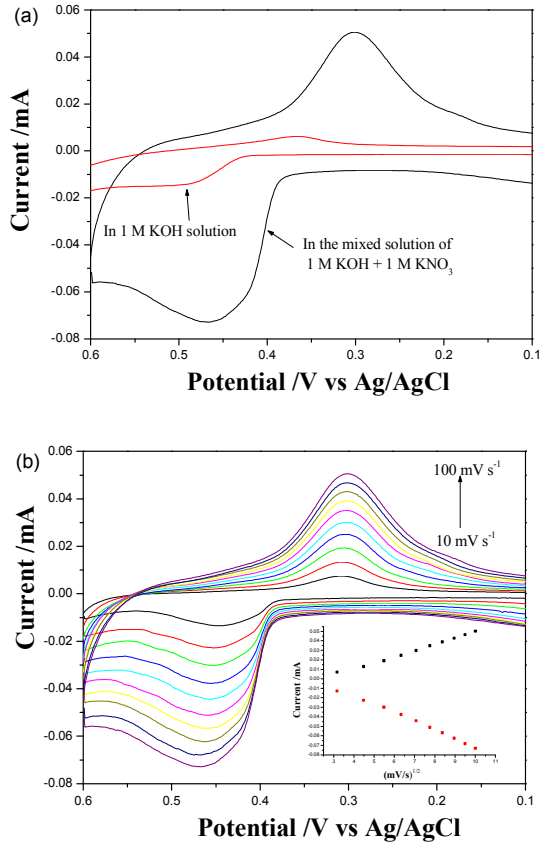

Figure 11 (a) Cyclic voltammograms (CVs) of Cu-Ni dendrites-modified GCE in a 1 M KOH solution and the mixed solution of 1 M KOH + 1 M KNO_3 at scan rate of 100 mV s^{-1}; (b) CVs of Cu-Ni dendrites-modified GCE in the mixed solution of 1 M KOH + 1 M KNO_3 at different scan rates (from inside to outside: 10, 20, 30, 40, 50, 60, 70, 80, 90, 100 mV s^{-1}). The inset in b is the linear relation between the peak currents and the square root of the scan rate.

Fig.12a depicts CVs of the bare GCE and the Cu-Ni modified GCE in 0.1 M KOH solution before and after adding 10 mM glucose. No obvious redox peak can be observed before and after adding 10 mM glucose when the bare GCE is used as the working electrode at the scan rate of 100 mV s^{-1}. After Cu-Ni modified GCE **is** used as the working electrode instead of the bare GCE, however, a pair of marked redox peaks **can** be found. Herein, different experimental phenomena **can** be observed before and after adding 10 mM glucose, which indicates an electrocatalytic oxidation process.[30,31] Namely, the as-obtained dendritic Cu-Ni microstructures **can** be used as a catalyst for the electrochemical oxidation of glucose in alkaline medium. **Fig.12b** displays the current-time plots for the present CuNi/Nafion/GCE at the oxidative potential of ~0.56 V with successive addition of glucose in 0.1 M KOH solution. The CuNi/Nafion/GCE rapidly **responds** to the changes of glucose concentration and steady state signal **is** obtained within 3 s. The linear relationship between the glucose concentration and the catalytic current is shown in the inset of **Fig.12b**. The detection limit is 0.098 M.

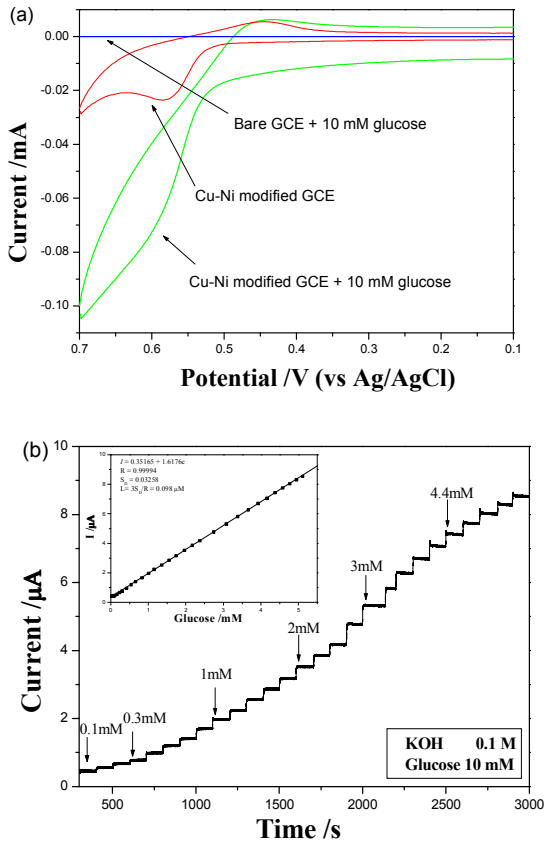

Figure 12 (a) the CVs of the bare GCE and the Cu-Ni modified GCE in 0.1 M KOH solution before and after adding 10 mM glucose; (b) Amperometric response of the CuNi/Nafion/GCE electrode upon the successive addition of glucose into 0.1 M KOH solution at 0.56 V. The inset is the linear relationship between the glucose concentration and the catalytic current.

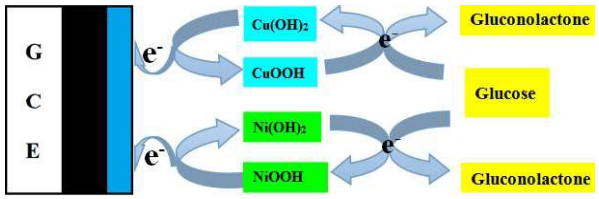

Scheme 1 the illustration of glucose electrocatalytic reaction mechanism.

Recently, Wang et al reported the preparation of reduced grapheme oxide-chitosan (RGO-CHIT) nanocomposites modified Cu-Co/GCE and application in the detection of

glucose.[32] They believed that Cu(0) and Co(0) were firstly transformed into $Cu(OH)_2$ and $Co(OH)_2$ in the alkaline conditions, and further electrochemically oxidized into CuOOH and CoO_2. Then, glucose was oxidized by CuOOH and CoO_2 into gluconolactone. In the present work, a similar redox process should also take place: In alkaline solution, Cu-Ni **microstructures** were firstly oxidized into $Cu(OH)_2$ and $Ni(OH)_2$, then further electrochemically oxidized into CuOOH and NiOOH. The produced CuOOH and NiOOH presented strong oxidative ability. Thus, glucose was oxidized into gluconolactone, and simultaneously $Cu(OH)_2$ and $Ni(OH)_2$ reappeared. The above process can be simply illustrated in Scheme 1.

4. Conclusions

In summary, dendritic Cu-M (M = Fe, Co and Ni) microstructures have been successfully obtained via a facile, environment-friendly, and rapid electrodeposited route in boric acid system at room temperature. It was found that the presence of M^{2+} salts caused the growth of dendritic microstructures under the current electrodeposited conditions. As a case, Cu-Ni dendrites were studied in detail to ascertain the factors affecting the formation of perfect Cu-M dendrites. Experiments uncovered that original amounts of $NiCl_2$ and boric acid were two main parameters affecting the morphology of dendritic Cu-Ni microstructures. Simultaneously, the higher deposition current and the longer deposition time were unfavourable to the growth of perfect dendrites. More importantly, the as-deposited Cu-M dendrites exhibited excellent catalytic activity for the reduction of 4-nitrophenol in excess $NaBH_4$ solution. The corresponding rate constants were calculated to be 0.83 min^{-1} for Cu-Ni, 0.69 min^{-1} for Cu-Fe and 0.48 min^{-1} for Cu-Co, respectively. Furthermore, Cu-Ni dendrites also owned excellent catalytic activity for the electrochemical reduction of NO_3^- ions to NH_3 in the alkaline medium, and were prepared into a sensor for the electrochemical detection of glucose in KOH solution with a detection limit of 0.098 M.

Acknowledgements

The authors thank the National Natural Science Foundation of China (21171005 and 21571005) for the fund support.

Notes and references

1 (a) Y.M. Zhang, Y.H. Ni, X.M. Wang, J. Xia, J.M. Hong, Cryst. Growth Des. 2011, 11, 4368-4377; (b) Y.H. Ni, X.X. Wang, J.M. Hong, RSC Adv., 2012, 2, 546-551; (c) J.J Xi, Y.H. Ni, A.M. Liu, New J. Chem. 2014, 38, 1738.
2 M. Hu, J.S. Jiang, X.D. Li, Cryst. Growth Des., 2009, 9, 820-824.
3 (a) M. Sanles-Sobrido, M. A. Correa-Duarte, S. Carregal-Romero, B. Rodríguez-González, R. A. Álvarez-Puebla, P. Hervés, L. M. Liz-Marzán, Chem. Mater. 2009, 21, 1531-1535; (b) J.X. Fang, H.J. You, P. Kong, Y. Yi, X.P. Song, B.J. Ding, Cryst. Growth Des. 2007, 7, 864-867.
4 H. Basu, K. M. Kolwankar, A. K. Dharmadhikari, J. A. Dharmadhikari, K. Bambardekar, S. Sharma, D. Mathur, J. Phys. Chem. C. 2012, 116, 11480-11485.
5 Z.P. Peng,Y.S. Jiang, Y.H. Song, Chem. Mater, 2008, 20, 3153-3162.
6 (a) Q.M. Shen, L.P. Jiang, H. Zhang, Q.H. Min, W.H. Hou, J.J. Zhu, J. Phys. Chem. C 2008, 112, 16385-16392; (b) C.L. Yan, D.F. Xue, Cryst. Growth Des. 2008, 8, 1849-1854.
7 L. Wang, Y. Yamauchi, Chem. Mater. 2009, 21, 3562-3569.
8 (a) X.M. Wang, Yonghong Ni, RSC Adv. 2012, 2, 2340-2345; (b) Y.H. Ni, Y.M. Zhang, J.M. Hong, CrystEngComm, 2011, 13, 934-940; (c) Y.H. Ni, Y.M. Zhang, J.M. Hong, CrystEngComm, 2011, 13, 1910. (d) Y.H. Ni, Y.M. Zhang, L. Zhang J.M. Hong, CrystEngComm, 2011, 13, 794-799.
9 (a) R. Qiu, J. Y. Zheng, H. G. Cha, M. H. Jung, K. J. Lee, Y. S. Kang, Nanoscale, 2012, 4, 1565; (b) R. K. Shervedani, M. Karevan, A. Amini, Sensors and Actuators B 2014, 204, 783-790; (c) K. Rumpf, P. Granitzer, N. Koshida, P. Poelt, M. Reissner, Nanoscale Res. Lett. 2014, 9, 412; (d) K.L. Wu, X.W. Wei, X.M. Zhou, D.H. Wu, X.W. Liu, Y. Ye, Q. Wang, J. Phys. Chem. C 2011, 115, 16268-1627.
10 (a) D.Q. Zhang, R.R. Wang, M.C. Wen, D. Weng, X. Cui, J. Sun, H.X. Li, Y.F. Lu, J. Amer. Chem. Soc. 2012, 134, 14283-14286; (b) A.R. Rathmell, S.M. Bergin, Y.L. Hua, Z.Y. Li, B.J. Wiley, Adv. Mater. 2010, 22, 2558; (c) J.C. Yu, F.G. Zhao, W. Shao, C.W. Ge, W.S. Li, Nanoscale, 2015, 7, 8811-8818.
11 S. Kang, M. Takeda, Z. Hiroi, G.W. Kim, C.G. Lee, B.H. Koo, J. Phys. D-Appl. Phys. 2010, 43, 415001.
12 I. E. Stewart, A. R. Rathmell, L. Yan, S.R. Ye, P. F. Flowers, W. You, B. J. Wiley, Nanoscale, 2014, 6, 5980.
13 A. Ungureanu, B. Dragoi, A. Chirieac, S. Royer, D. Duprez, E. Dumitriu, J. Mater. Chem., 2011, 21, 12529.
14 T. Wu, W.Y. Cai, P. Zhang, X.F. Song, L. Gao, RSC Adv., 2013, 3, 23976.
15 Q.X. Wu, W. L. Eriksen, L. D. L. Duchstein, J. M. Christensen, C. D. Damsgaard, J. B. Wagner, B. Temel, J.-D. Grunwaldtae, A. D. Jensen, Catal. Sci. Technol., 2014, 4, 378.
16 S.H. Pang, N.E. Love, J. W. Medlin, J. Phys. Chem. Lett. 2014, 5, 4110-4114.
17 H. Liu, Ch.Y. Guan, X. Li, L.Y. Cheng, J.B. Zhao, N.H. Xue, W.P. Ding, ChemCatChem, 2013, 5, 3904-3909.
18 L. Mattarozzi, S. Cattarin, N. Comisso, A. Gambirasi, P. Guerriero, M. Musiani1, L. Vázquez-Gómez, E. Verlato, Electrochimica Acta 2014, 140, 337-344.
19 L. Mattarozzi, S. Cattarin, N. Comisso, P. Guerrierob, M. Musiania, L. Vázquez-Gómez, E. Verlato, Electrochimica Acta 2013, 89, 488-496.
20 J. Zhang, M. D. Baró, E. Pellicer, J. Sort, Nanoscale, 2014, 6, 12490.
21 Ö.F. Bakkaloğlu, İ.H. Karahan, H. Efeoğlu, M. Yıldırım, U. Çevik, Y.K. Yoğurtcu, J. Mag. Mag. Mater. 1998, 190, 193-198.
22 R. Pattanayak, S. Panigrahi, T. Dash, R. Muduli, D. Behera, Physica B., 2015, 474, 57–63.
23 I.S. Zhidkov, N.A. Skorikov, A.V. Korolev, A.I. Kukharenko, E.Z. Kurmaev, V.E. Fedorov, S.O. Cholakh, Carbon, 2015, 91, 298–303.
24 R. Souchet, F. Danoix, A. D'Huysser c, M. Lenglet, Applied Surface Science, 1995, 87/88, 271-278.
25 (a) Y.H. Ni, Y.M. Zhang, J.M. Hong, Cryst. Growth Des. 2011, 11, 2142-2148; (b) G. R. Li, C.Z. Yao, X.H. Lu, F.L. Zheng, Z.P. Feng, X.L. Yu, C.Y. Su, Y.X. Tong, Chem. Mater. 2008, 20, 3306-3314.
26 M. Supicova, R. Rozik, L. Trnkova, R. Orinakova, M. Galova, J. Solid State Electrochem., 2006, 10, 61.
27 L. M. Graham, S. Cho, S. K. Kim, M. Noked, S. B. Lee, Chem. Commun., 2014, 50, 527.
28 A. Brenner, Electrodeposition of alloys: principles and practice, 1963, volume 1, Academic press, New York and London, p.77-78.
29 (a) C. L. Yan, D. F. Xue, Cryst. Growth Des. 2008, 8, 1849-1854; (b) W. Che, Y.H. Ni, Y.X. Zhang, Y. Ma, J. Phys. Chem. Solids, 2015, 77, 1–7.
30 F.F. Yuan, Y.H. Ni, L. Zhang, S.M. Yuan, J.D. Wei, J. Mater. Chem. A, 2013, 1, 8438-8444.
31 L. Zheng, J. Q. Zhang, J. F. Song, Electrochim. Acta 2009, 54, 4559.
32 L. Wang, Y.L. Zheng, X.P. Lu, Z. Li, L.L. Sun, Y.H. Song, Sensors and Actuators B 2014, 195, 1-7.